8-1995

Comparison of Time-domain Reflectometry Performance Factors for Several Dielectric Geometries: Theory and Experiments

S. V. Maheshwarla
University of Nevada, Las Vegas

R. Venkatasubramanian
University of Nevada, Las Vegas

Robert F. Boehm
University of Nevada, Las Vegas, bob.boehm@unlv.edu

WATER RESOURCES RESEARCH, VOL. 31, NO. 8, PAGES 1927–1933, AUGUST 1995

Comparison of time domain reflectometry performance factors for several dielectric geometries: Theory and experiments

S. V. Maheshwarla and R. Venkatasubramanian
Department of Electrical and Computer Engineering, University of Nevada, Las Vegas

Robert F. Boehm
Department of Mechanical Engineering, University of Nevada, Las Vegas

Abstract. We propose three nontraditional dielectric geometries and present an experimental and theoretical analysis and comparison of time domain reflectometry (TDR) performances for them. The traditional geometry (the probes inserted in material of essentially infinite extent) is compared to three nontraditional geometries where the probes are affixed outside of a core sample, inside of a bore, or flat on the surface of a semi-infinite solid. Our derivation relates the velocity of electromagnetic wave propagation to the complex permittivities and permeabilities of the media and the geometry for the three nontraditional configurations. Experimental results for air, styrofoam, dry sand, wet sand of varying water content, nylon, dry wood, and ferromagnetic steel are obtained for the three proposed configurations and are in fair agreement with the literature within the experimental uncertainties. Through experiments and theoretical analysis, the TDR performance is found to be the same within the experimental uncertainties for the three nontraditional geometries. The proposed geometries yield slightly lower sensitivities compared to the traditional geometry. Advantages and disadvantages of the geometries compared to the traditional geometry are also discussed.

1. Introduction

In the 1970s broadband VHF and UHF transmission line methods were developed for characterizing materials based on their dielectric and magnetic properties [*Bussey*, 1967; *Chudobiak et al.*, 1979a, b; *Van Beck*, 1965]. Some of the possible geometries are completely embedded parallel bar balanced open transmission lines, partially embedded open parallel plate transmission lines, and completely embedded unbalanced coaxial transmission lines [*Chudobiak et al.*, 1979b]. The relationships between the complex permittivities and permeabilities and the dimensions of the transmission, the characteristic impedance, and the velocity of propagation for all the above discussed geometries are presented by *Chudobiak et al.* [1979a, b]. Several materials, moist soil, concrete, asphalt, moist paper, and Plexiglas have been characterized based on the transmission line technique in the frequency range of 10–1000 MHz [*Chudobiak et al.*, 1979a, b].

In the last decade, time domain reflectometry (TDR) has become one of the primary tools for measuring water content in soil [*Topp et al.*, 1980]. The first report of *Topp et al.* [1980] showed that TDR is a powerful tool to measure water content in soil. In a later study, *Topp et al.* [1982] showed that by introducing convenient discontinuities in the geometry of the transmission line, water content depth profiles can be obtained. Recently, three-wire and four-wire transmission lines have been proposed and demonstrated to overcome the difficulties arising from the change of the transmission line from an unbalanced coaxial line to a matched twin-lead line [*Zegelin et al.*, 1989]. In a recent noninvasive TDR technique [*Selker et al.*, 1993] the probes are placed on the surface of the wet sand and are demonstrated to be useful for soil water content measurement. However, the dielectric constants at a given water content are about one half that reported by *Topp et al.* [1980]. In a recent experimental study, *Xu et al.* [1993] have demonstrated a noninvasive TDR technique for unsaturated flow experiments. *Knight et al.* [1994] have discussed a surface probe with the probe placed in between two dielectric media and proposed a possible relationship to infer the permittivities of the media.

In most of the above mentioned studies, the soil completely surrounded the transmission line probes. In this paper we propose three new nontraditional geometric arrangements of probe conductors in two different media with varying dielectric and magnetic properties which are suitable for TDR measurements. The proposed geometries naturally exist in many engineering situations such as mines and tunnels used in geologic studies. These geometries can also be intentionally created if they will not interfere with the physics of the problem of study. The performance factor of the three nontraditional geometries is compared with that of the traditional geometry where the two probes are inserted a fixed distance apart in an infinite medium.

This paper is organized as follows. In section 2 the three nontraditional probe geometries are proposed. The transmission line problem related to one of the geometries is addressed. An analytical relationship is developed between the velocity of propagation of an electromagnetic wave in the media and characteristics including permittivity and permeability and geometric parameters such as the distance between the probes and the radii of the probes. In section 3, experimental results for various combinations of dielectric and magnetic media are presented and compared with the available data.

Paper number 95WR00788.
0043-1397/95/95WR-00788$05.00

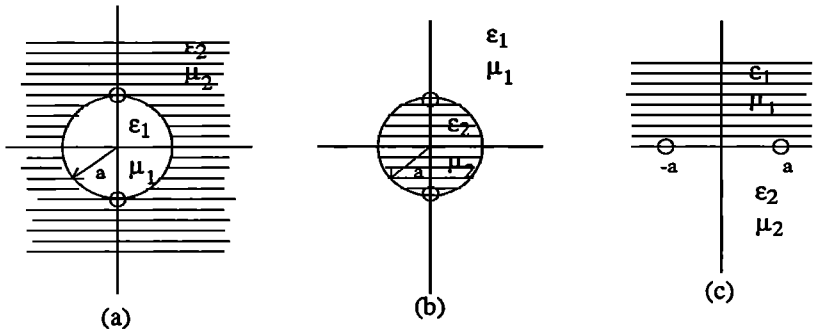

Figure 1. Three nontraditional geometries of arrangement of the two media. The small circles represent conducting probes.

The performance factors of the three proposed geometries are compared with the traditional one using experiments and a theoretical analysis. Conclusions are presented in section 4.

2. Nontraditional Geometries and Their Electromagnetics

2.1. Geometric Configuration

The three nontraditional geometries are shown in Figure 1. Figure 1a describes the geometry in which the probes are placed at diametrically opposite points of a circular core sample of radius a whose electrical and magnetic properties are different from that of the surrounding medium (geometry 1). Figure 1b is similar to Figure 1a, except that the media are interchanged (geometry 2). Figure 1c describes the geometry which consists of two semi-infinite media with the probes being placed at the interface between the media at a distance of $2a$ apart (geometry 3).

Let us the consider the geometry 1 as shown in Figure 1a and obtain the relationship between the velocity and the properties and geometry of the media. Denote the permittivity and permeability of the infinite medium as ε_2 and μ_2, respectively. Further, denote the permittivity and permeability of the circular medium as ε_1 and μ_1, respectively. In general, the permittivity can be treated as complex with the form

$$\varepsilon = \varepsilon' - j\varepsilon'' \tag{1}$$

where ε' and the ε'' are the real and imaginary parts of the permittivity with the imaginary part representing the loss in the medium. Similarly, the permeability can be treated as complex with the form

$$\mu = \mu' - j\mu'' \tag{2}$$

where μ' and the μ'' are the real and imaginary parts of the permeability, with the imaginary part representing the magnetic losses in the medium.

2.2. Electromagnetic Problem and Its Solution

Let the probes of a twin-lead transmission line be placed at the interface between the media at diametrically opposite ends on the y axis as shown in Figure 1. Note that the the interface is the x axis and the small circles represent the probes. The velocity of propagation of an electromagnetic wave in the inhomogeneous media, v, is related to the capacitance, C, and inductance, L, of the transmission line as

$$v = 1/(LC)^{1/2} \tag{3}$$

where C and L are assumed frequency independent. To obtain the velocity of propagation for the three geometries discussed in section 2, the capacitance and inductance of the transmission line should be related to the permittivities, permeabilities, and geometries.

Conformal mapping of the geometry using the following transformation was performed to make it amenable to a simple solution:

$$z = x + iy$$

$$= a\left(\frac{i - w}{i + w}\right) \tag{4}$$

where a is the radius of the second medium and $w = u + iv$. The reverse transformation results in

$$u = \frac{2ay}{(x + a)^2 + y^2} \tag{5}$$

$$v = \frac{a^2 - x^2 - y^2}{(x + a)^2 + y^2} \tag{6}$$

Pictorially, the transformation is shown in Figure 2. The geometry shown in the w plane in Figure 2 is amenable to easy solution.

2.3. Capacitance of the Line

With Gauss law and appropriate field boundary conditions, the electric field due to the $+Q$ located on the probe at $(a, 0)$, as shown in Figure 2, can be shown to be

$$\mathbf{E}_+(u, 0) = \frac{-Q}{\pi(1 - u)(\varepsilon_1 + \varepsilon_2)}\,\mathbf{a}_u \tag{7}$$

where $\mathbf{a}_u$ is the unit vector along the u direction. Similarly the electric field due to the $-Q$ on the probe at $(-a, 0)$ can be shown to be

$$\mathbf{E}_-(u, 0) = \frac{-Q}{\pi(1 + u)(\varepsilon_1 + \varepsilon_2)}\,\mathbf{a}_u \tag{8}$$

From (7) and (8) we get the total electric field, $\mathbf{E}_{\text{tot}}(u, 0)$ as

$$\mathbf{E}_{\text{tot}}(u, 0) = \mathbf{E}_+(u, 0) + \mathbf{E}_-(u, 0)$$

$$= \frac{-Q}{\pi(\varepsilon_1 + \varepsilon_2)}\left[\frac{1}{1 - u} + \frac{1}{1 + u}\right]\mathbf{a}_u \tag{9}$$

Noting that the potential difference between the probes, V_{AB}, is independent of path, we get an expression for V_{AB} as

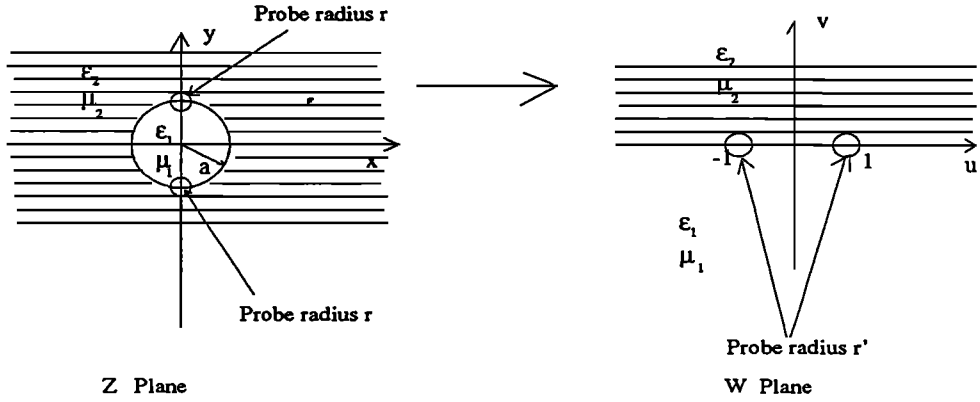

Figure 2. Conformal transformations $z \rightarrow w$ and resulting change in the geometry. Note that the probe radii change from r to r'.

$$V_{AB} = -\int_{-1+r'}^{1-r'} \mathbf{E}_{\text{tot}}(u, v) \cdot \mathbf{dl} \tag{10}$$

$$V_{AB} = \int_{-1+r'}^{1-r'} \frac{Q}{\pi(\varepsilon_1 + \varepsilon_2)} \left[\frac{1}{1-u} + \frac{1}{1+u}\right] du \tag{11}$$

$$V_{AB} = \frac{Q}{\pi(\varepsilon_1 + \varepsilon_2)} \log\left(\frac{2-r'}{r'}\right)^2 \tag{12}$$

where r' is the radius of the probe in the w plane along the u direction. Equation (12) is strictly true only when $r' \ll 2$. Using (12), the capacitance per unit length, C in the z plane, is given by

$$C = \left(\frac{\pi(\varepsilon_1 + \varepsilon_2)}{\log\left(\frac{2a-r}{r}\right)^2}\right) \tag{13}$$

where the terms 2 and r' (w plane) in the logarithmic term of (12) transform to $2a$ and r, respectively, in (13) (z plane). Note that the ε_1 and ε_2 can be treated as complex if the dielectric media are lossy. Equation (13) shows that the transmission line for geometry 1 can be modeled as two capacitors in parallel connection as shown in Figure 3. Under the condition that $\varepsilon_1 = \varepsilon_2$, the capacitance per unit length given by (13) reduces to that of a twin-lead transmission line with a homogeneous dielectric medium [*Liboff and Dalman*, 1931]. Since the capacitance given by (13) is symmetric in ε_1 and ε_2, it is obvious that (13) applies to geometry 2 as well. The above derivation shows that the inner cylindrical core material and the surrounding infinite medium play equally important roles in deciding the capacitance of the line. Capacitance for geometry 3 can be evaluated from (12) by assuming $r' = r$, which yields (13). Thus the three proposed geometries are identical in terms of the capacitance of the line.

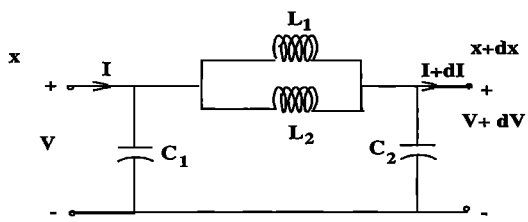

Figure 3. An equivalent transmission line model showing parallel capacitors and parallel inductors.

2.4. Inductance of the Line

Using an approach similar to that employed in section 2.3, with Ampere law and appropriate boundary conditions for the magnetic fields, the total magnetic flux density, $\mathbf{B}_{\text{tot}}(\mathbf{u})$ can be obtained as

$$\mathbf{B}_{\text{tot}}(u, 0) = \mathbf{B}_{+}(u, 0) + \mathbf{B}_{-}(u, 0)$$

$$= \frac{-I}{\pi} \frac{\mu_1\mu_2}{\mu_1 + \mu_2} \left[\frac{1}{1-u} + \frac{1}{1+u}\right] \mathbf{a}_u \tag{14}$$

Noting that the magnetic flux between the probes per unit length, ϕ_{tot}, is independent of path, we get an expression for ϕ_{tot} as

$$\phi_{\text{tot}} = \int_{-1+r'}^{1-r'} \mathbf{B}_{\text{tot}}(u, v) \cdot \mathbf{dl} \tag{15}$$

$$\phi_{\text{tot}} = \int_{-1+r'}^{1-r'} \frac{I(\mu_1\mu_2)}{\pi(\mu_1 + \mu_2)} \left[\frac{1}{1-u} + \frac{1}{1+u}\right] du \tag{16}$$

$$\phi_{\text{tot}} = \frac{I(\mu_1\mu_2)}{\pi(\mu_1 + \mu_2)} \log\left(\frac{2-r'}{r'}\right)^2 \tag{17}$$

where r' is the transformed radius of the probe in the w plane along the u direction. Equation (17) is strictly true only when $r' \ll 2$. Using (17), the inductance per unit length, L, in the z plane, can be shown to be

$$L = \left(\frac{\mu_1\mu_2}{\pi(\mu_1 + \mu_2)}\right) \log\left(\frac{2a-r}{r}\right)^2 \tag{18}$$

The integration approach here is similar to that performed to obtain the capacitance. Note that the μ_1 and μ_2 can be treated as complex if the dielectric media are lossy. Equation (18) shows that the transmission line shown in Figure 2 can be modeled as two inductors in parallel connection as shown in Figure 3. Under the condition that $\mu_1 = \mu_2$, the inductance per unit length given by (18) reduces to that of a twin-lead transmission line with a homogeneous magnetic medium [*Liboff and Dalman*, 1931]. Symmetry arguments presented in section 2.3

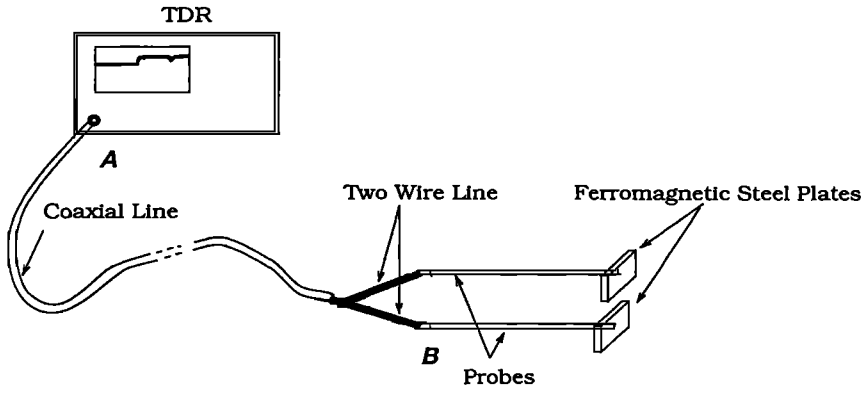

Figure 4. A schematic TDR setup showing the coaxial line, the two-wire line, and the brass probes.

can be extended to (17) and (18), which show that (18) applies to all three geometries. Moreover, it is found that the inner core material and the surrounding medium play equally important roles in deciding the inductance of the line.

2.5. Velocity of Propagation

Using (13) and (18), the velocity of propagation of an electromagnetic wave along the transmission line given by (3) for the three geometries can be written as

$$v = \mathrm{Re}\left\{\left[\left(\frac{\mu_1 + \mu_2}{\mu_1\mu_2}\right)\left(\frac{1}{(\varepsilon_1 + \varepsilon_2)}\right)\right]^{1/2}\right\} \qquad (19)$$

In the above equation, in general, $\varepsilon_1 = \varepsilon_1' - j\varepsilon_1''$, $\varepsilon_2 = \varepsilon_2' - j\varepsilon_2''$, $\mu_1 = \mu_1' - j\mu_1''$, and $\mu_2 = \mu_2' - j\mu_2''$, where the double prime terms represent the lossy nature of the media. Equation (19) shows that the solution for these geometries is the solution of a transmission line with two capacitors and two inductors all in parallel combination with each capacitor and inductor combination representing the inner core material and the infinite medium. Equation (19) also shows that in the limit $\mu_1 = \mu_2$ and $\varepsilon_1 = \varepsilon_2$, this case reduces to the solution of a homogeneous transmission line [*Liboff and Dalman*, 1931].

3. Results

In this section we present results confirming the validity of the analytical expression given by (19) through TDR experiments using a variety of dielectrics and magnetic materials. Additionally, we present results of water content measurement of wet soil using geometry 1 and compare it to reinterpreted literature data [*Selker et al.*, 1993] of geometry 3. Also, a theoretical analysis of the sensitivities of the proposed geometry and the traditional geometry is performed, and the sensitivities are compared.

3.1. Experiments

A Tektronix model 1502 C cable tester was employed for experiments. The coaxial line from the output of the TDR was soldered to a two-wire line, and the two-wire line was connected to two brass probes of 2.5 mm diameter and 30 cm length. The brass probes were placed at diametrically opposite ends of the inner cylindrical medium. Thus the distance between the probes was always equal to the diameter of the inner cylindrical medium. A schematic picture of the setup is shown in Figure 4.

Owing to multiple reflections of the electromagnetic wave at the various junctions resulting from the impedance changes, it is hard to relate the displayed signal and the corresponding point along the probes. To counter this problem, the following technique was followed to accurately relate the signal and the point along the probe. Steel plates measuring 5 × 5 × 0.5 cm (with high magnetic permeability, $\mu = 5000\mu_0$) with a central hole were placed at the two ends of both the probes. The presence of a highly permeable medium such as steel presents an impedance to the electromagnetic wave, and therefore a dip in the TDR signal is expected. A typical TDR scan for geometry 2 with the ferromagnetic steel plates placed at the end of the probe is shown in Figure 5. Even though the approximate location corresponding to the ferromagnetic plate can be obtained by accounting for each discontinuity in the signal as a discontinuity in the TDR probe, the exact location is hard to find. The dip in the signal denoted as a cross in Figure 5 was found by a series of experiments to correspond to the position of the ferromagnetic plate. The experiments consisted of moving the ferromagnetic plate an elemental distance and observing the location along the scan at which the signal registers the maximum change. By performing numerous experiments with various media, it was found that the location of the start of the probe is a fixed value on the length scale of the TDR and is independent of the media between and surrounding the probes. This is expected as the TDR distance from the output of the TDR (A in Figure 4) to the start of the probe (B in Figure 4) is dictated primarily by the coaxial line and the two-wire lines so long as the electrical and magnetic properties of the media in between are kept unchanged. Thus it is sufficient to use two steel plates, one at each end of the probes.

Two sets of experiments, measurement of permittivities and

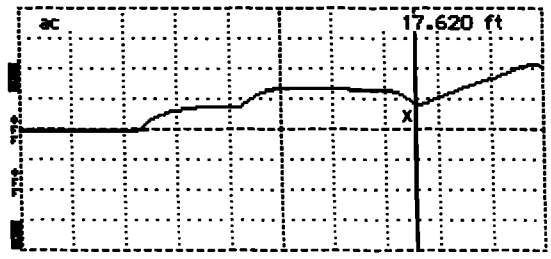

Figure 5. A TDR scan for the geometry 2 showing the discontinuities in the signals. Note that the dip denoted with a cross corresponds to the position of the ferromagnetic plates placed at the end of the probes. (1 foot equals 0.3048 m.)

Table 1. Measured Values and Literature Data for Relative Permittivities of Sand (κ_{san}), Styrofoam (κ_{sty}), Nylon (κ_{nyl}), and Dry Wood (κ_{woo})

Interprobe Distance, cm	Geometry 1: Medium 1/Medium 2	Assumed Relative Permittivity Used in (21)	Calculated Relative Permittivity of Unknown Medium	Relative Permittivity From the Literature With Reference
10	styrofoam/styrofoam	...	$\kappa_{sty} = 1.275$	1.03* [*Liao*, 1988]
20	styrofoam/styrofoam	...	$\kappa_{sty} = 1.27$	1.03* [*Liao*, 1988]
10	dry sand/styrofoam†	$\kappa_{sty} = 1.3$	$\kappa_{san} = 2.728$	2.8 [*Liao*, 1988]
20	dry sand/styrofoam†	$\kappa_{sty} = 1.3$	$\kappa_{san} = 2.642$	2.8 [*Liao*, 1988]
30	dry sand/styrofoam†	$\kappa_{sty} = 1.3$	$\kappa_{san} = 3.025$	2.8 [*Liao*, 1988]
5	nylon/air	$\kappa_{air} = 1.0$	$\kappa_{nyl} = 2.85$	3.6 at 1 MHz‡, [*NYTEF Company*, 1994]
5	hard dry wood/air	$\kappa_{air} = 1.0$	$\kappa_{woo} = 2.98$	1.5–4.0‡ [*Liao*, 1988]
10	styrofoam/air	$\kappa_{air} = 1.0$	$\kappa_{sty} = 1.55$	1.03* [*Liao*, 1988]

Note that $\kappa_i = \varepsilon_i/\varepsilon_0$ where ε_0 is the permittivity of free space.
*Permittivity of styrofoam depends on the density.
†For our experiments with styrofoam as the material with known permittivity, we have used the permittivity of styrofoam from our measurements owing to the consistency of the values for all four geometries, including the traditional geometry.
‡Permittivities of wood and nylon are dependent on the frequency of the electromagnetic signal and the specific form of the material.

permeabilities of various dielectric and magnetic materials (experiment 1), and measurement of permittivity of soil as a function of water content (experiment 2), were performed. Details of the experiments and the results are presented and discussed below.

3.1.1. Experiment 1. Dielectric and magnetic materials of a cylindrical shape or with a cylindrical hole in them were employed to study their permittivities and permeabilities. The media considered were air, dry sand, low-density styrofoam, ferromagnetic steel, nylon, and dry wood. Owing to the limitations of some of the materials, only some of the configurations could be tested. Note that the effective permittivity of the media is an arithmetic mean of the permittivities of the two media and the effective permeability is a harmonic mean of the permeabilities of the media. The TDR experiments yield relative velocity of the electromagnetic wave in the media to that of air, v_{media}/v_{air}. The relative velocity is directly related to the effective permittivities and permeabilities of the media as

$$\left(\frac{v_{media}}{v_{air}}\right)^2 = \frac{\varepsilon_0\mu_0}{\varepsilon_{eff}\mu_{eff}} \tag{20}$$

with $\mu_{eff} = 2\mu_1\mu_2/(\mu_1 + \mu_2)$ and $\varepsilon_{eff} = (\varepsilon_1 + \varepsilon_2)/2$. Consider the TDR results of a combination of two nonmagnetic dielectric media. Equation (20) will simplify to

$$\left(\frac{v_{media}}{v_{air}}\right)^2 = \frac{\varepsilon_0}{\varepsilon_{eff}} = \frac{2\varepsilon_0}{\varepsilon_1 + \varepsilon_2} \tag{21}$$

To infer the permittivity of one of the medium from (21), one needs to know the permittivity of the other medium. A similar argument holds for the permeability also.

The results of our measurements of relative velocity along with (19) were employed to obtain the permittivities and permeabilities of various dielectric and magnetic materials and are reported in Table 1. The known permittivity listed in the "assumed relative permittivity" of Table 1 is assumed to infer the permittivity of the unknown material. These results were compared with experimental data reported in the literature [*Liao*, 1988; *NYTEF Company*, 1994]. Fairly good agreement obtained as shown in Table 1 establishes the validity of equations (13), (18), and (19) within the experimental uncertainties such as the influence of frequency, temperature, and humidity on the dielectric and magnetic properties of the materials, the error in interpreting the TDR scan, and the possibility of excitation of nontransverse waves. Experiments with a 15-cm-long and 5-cm-diameter ferromagnetic steel rod (covered with electrical insulation) yielded a velocity of about 1.4 times that of air, which by (20) results in $\mu_{steel} \gg \mu_0$, which is in agreement with [*Liao*, 1988]. It is noted that the data reported in [*Liao*, 1988] are frequency, temperature, humidity, and the history of the material and the TDR employs a rectangular pulse which contains many frequency components. Therefore any comparison of the results should be made with caution.

3.1.2. Experiment 2. For the purpose of this experiment, a 120 × 120 × 60 cm low-density styrofoam block was used with circular through cuts of diameters 10, 20, and 30 cm along the thickness direction. The concentric cylindrical pieces were preserved and employed during the experiments. A schematic picture of the block is shown in Figure 6. By removing the inner pieces one by one, the diameter of the hole in the styrofoam can be changed from 10 to 20 to 30 cm. Since the probe length was 30 cm, a circular styrofoam block of diameter 30 cm was placed at a distance of 30 cm from the bottom as illustrated in Figure 6. The reason for limiting the hole length to 30 cm, even though 60 cm could have been used, is for ease of the experiment and economy of sand. (Unfortunately, the annular

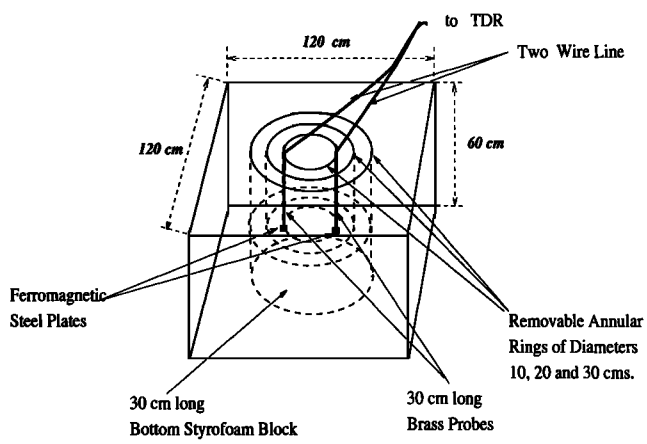

Figure 6. A schematic styrofoam block configuration used for the wet soil experiment.

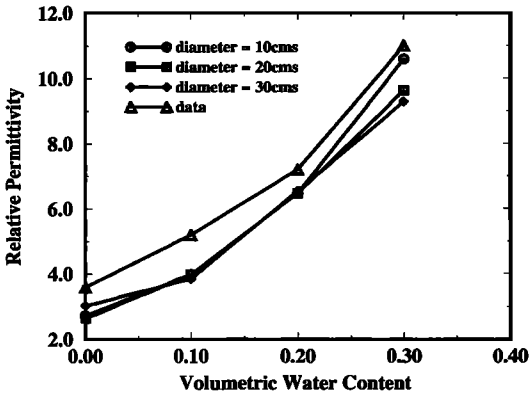

Figure 7. Permittivity of wet soil versus water content (by volume) from our experiments and reinterpreted from *Selker et al.* [1993].

pieces could not be cut to 30 cm due to difficulties in scooping out the bottom without destroying the annular pieces.) The probe end with the steel plate was made to exactly rest on the bottom styrofoam block and the probes were placed at diametrically opposite ends of the inner hole. Then the hole was filled with sand with varying contents of tap water. Four sets of experiments with three interprobe distances were performed and the results were obtained. The results for 0%, 10%, 20% and 30% (by volume) water contents are shown in Figure 7. The relative permittivity of styrofoam was assumed to be 1.3 (data from our experiments with four geometric configurations). The results are consistent among themselves and are in fairly good agreement with the literature [*Topp et al.*, 1980; *Selker et al.*, 1993].

3.2. Theoretical Analysis

Using a theoretical analysis, let us compare the sensitivities to permittivity variation of these three geometries to that of the traditional geometry. Since the three geometries result in the same relationships and hence the same sensitivity to moisture content, let us consider the geometry 1 as shown in Figure 1a. Let the radius of the circular hole be a. The hole contains air and, therefore, its $\varepsilon_1 = \varepsilon_0 = 8.85 \times 10^{-12}$ F/m. Let us vary the ε_2 and plot the velocity given by (19). It is assumed that $\mu_1 = \mu_2 = \mu_0 = 4\pi \times 10^7$ H/m. For this case, (19) reduces to

$$v = \left(\frac{2}{(\varepsilon_0 + \varepsilon_2)(\mu_0)}\right)^{1/2} \tag{22}$$

A plot of v versus ε_2 is shown in Figure 8, showing that the ε_2 varies with moisture content [*Topp et al.*, 1980]. Consider the traditional application and let the permeability be ε_2 (soil with varying water content) and $\mu_1 = \mu_2 = \mu_0 = 4\pi \times 10^7$ H/m. Equation (22) for this case reduces to

$$v = \left(\frac{1}{(\varepsilon_2)(\mu_0)}\right)^{1/2} \tag{23}$$

A plot of v versus ε (soil with varying water content) is shown in Figure 8. From Figure 8 it is obvious that the geometry 1 is of comparable sensitivity to the traditional application.

3.3. Reinterpretation of Literature Data

The geometric configuration proposed by *Selker et al.* [1993] is similar to that of our geometry 3, except for the presence of the thin acrylic material. In the absence of the acrylic material in their configuration, the velocity of propagation of an electromagnetic wave along the probe placed at the interface between two semi-infinite media should follow (19). Thus the effective dielectric constant, ε_{eff} reported by *Selker et al.* [1993], in actuality, satisfies the following condition:

$$\varepsilon_{\text{air}} + \varepsilon_{\text{wet soil}} = 2(\varepsilon_{\text{eff}}) \tag{24}$$

assuming that the acrylic is thin and plays a minor role in the propagation of electromagnetic waves. Data from Figure 2 of *Selker et al.* [1993] were reinterpreted using (24) and are presented along with our data for geometric configurations 1 and 2 in Figure 7. The good agreement between the data again establishes the validity of the (13), (18), and (19). It is noted that there is a constant shift of about 1.0 in the relative permittivity for the data of *Selker et al.* [1993] which is due to neglecting the acrylic materials whose high-frequency relative permittivity is approximately 2.7. Thus, if a relative permittivity between 1.0 and 2.7, for example, 2.0, is used in (24), the agreement between our data and those of *Selker et al.* [1993] will be excellent. It is noted that the present theory can only be used for obtaining semiquantitative behavior for the configuration presented by *Selker et al.* [1993]. Since the configuration of *Selker et al.* [1993] is theoretically very complicated, and because of the added uncertainties from experiments, the approach of obtaining calibration curves and utilizing them is the best approach [*Selker et al.*, 1993].

4. Discussion

It is shown that the velocity of electromagnetic wave propagation for three proposed geometries is related to the electrical and magnetic properties and the geometry through an analytical expression. The validity of the analytical expression is established through measurement of permittivities and permeabilities of various materials with known properties within experimental uncertainties such as signal interpretation, variation of properties with frequency, temperature, and humidity, and the possibility of excitation of nontransverse waves. Experimental studies on sand with varying water content have shown that the proposed configurations can be used for water content measurement of soil in cases where a hole already exists in the soil or where one can be drilled without affecting the flow characteristics. The comparative numerical study pre-

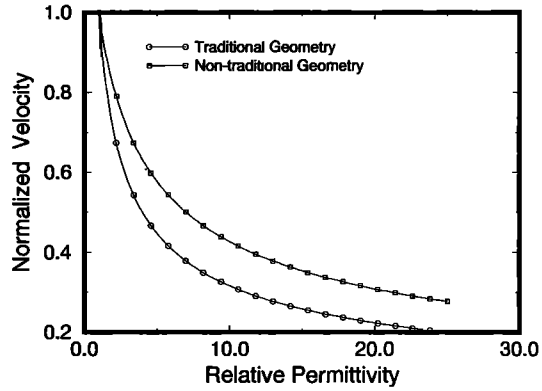

Figure 8. Relative permittivity $\varepsilon_2/\varepsilon_0$ versus v for the three proposed nontraditional geometries shown in Figure 1 and the traditional geometry.

sented in section 3.2 shows that the proposed geometries are of comparable sensitivity to the traditional geometry. Even though the traditional geometry is more sensitive to moisture content, owing to field constraints it may not be possible or desirable to install the probes into the medium. In such a case, geometry 3 can be adopted. For those cases where a hole, tunnel, or mine already exists, geometries 1 and 2 are more suitable than the traditional geometry or geometry 3.

The proposed geometries have several advantages over the traditional geometry for permittivity and permeability measurements. First, in many media (semi-infinite), drilling holes may not be desirable or possible, in which case the traditional geometry and geometries 1 and 2 cannot be used and geometry 3 is suitable. In cases of materials which exist or are produced in cylindrical form, the traditional geometry and the third proposed geometry are not suitable, whereas geometries 1 and 2 will be suitable. Second, instead of leaving the probe end open as is the standard practice in the traditional methods, it can be shorted for the proposed geometries. This will not only provide mechanical strength to the transmission line system, but also help in maintaining the distance between the probes constant throughout the measurement.

The limitations of the proposed geometries are as follows. First, intentionally forming a hole for the purpose of this measurement may interfere with fluid flow characteristics of the soil. But if the depth profile information is not needed, then geometry 3, which obviates the need for a hole, can be employed. Second, digging a hole for the purpose of this measurement is destructive and may not always be possible or desirable. Third, if the probes are too far apart and the input signal is weak, the TDR output will be weak. In this case, none of the proposed geometries is suitable. Also, these configurations are not suitable if the interprobe distance and the probe radii are of comparable dimension. It was found by experimentation with the instrumentation and the transmission line system described in section 3.1 that for an interprobe distance greater than 30 cm, the signal is weak and the error in the measurement is greater. It is noted that the experiments performed under this study are controlled laboratory experiments. Before these geometries are used in the field, field experimentation needs to be performed.

Use of a ferromagnetic steel plate to correlate the location along the probe to the distance scale on the TDR probe is unique to this study. Any material which provides high impedance to the electromagnetic wave, such as ferroelectric or ferromagnetic or ferrimagnetic materials, will be equally suitable.

5. Conclusion

We have proposed three nontraditional geometries for TDR characterization of various media. We have shown that the velocity of the TDR signal is related to the permittivities and permeabilities of the media through an analytical expression, if the media are homogeneous. The validity of the analytical expression is established by experimental measurement of permittivities and permeabilities of various media with known properties. It is also shown by experimentation that the proposed nontraditional geometries can be employed for water content measurement in soil. It is shown by a theoretical analysis that the TDR applications with the proposed geometries are comparably sensitive to variation in permittivity to the traditional geometry. It is believed that in applications where a hole or tunnel already exists, one of the geometries proposed, that is, as shown in Figure 1a, is the most suitable nondestructive technique to obtain property profiles of the matter surrounding the tunnel. If digging a hole is undesirable and the depth profile is not needed, then geometry 3 is the most suitable one.

Acknowledgment. The authors would like to gratefully acknowledge the constructive criticisms of the anonymous reviewers.

References

Bussey, H. E., Measurement of RF properties of materials—A survey, *Proc. IEEE, 55*, 1046–1053, 1967.

Chudobiak, W. J., M. R. Beshir, and J. S. Wright, An open transmission line UHF CW phase technique for thickness/dielectric constant measurement, *IEEE Trans. Instrum. Meas., IM-28*, 18–25, 1979a.

Chudobiak, W. J., B. A. Syrett, and H. M. Hafez, Recent advances in broad-band VHF and UHF transmission line methods for moisture content and dielectric constant measurement, *IEEE Trans. Instrum. Meas., IM-28*, 284–289, 1979b.

Knight, J. H., I. White, and S. J. Zeglin, Sampling volume of TDR probes for water content monitoring, in *Proceedings of Symposium and Workshop on Time Domain Reflectometry in Environmental, Infrastructure and Mining Applications*, pp. 93–104, Bur. of Mines, U.S. Dep. of Inter., Denver, Colo., 1994.

Liao, S., *Engineering Applications of Electromagnetics*, 422 pp., West, St. Paul, Minn., 1988.

Liboff, R. L., and G. C. Dalman, *Transmission Lines, Wave Guides and Smith Charts*, pp. 31–32, McGraw-Hill, New York, 1931.

NYTEF Company, Manufacturer catalog, New York, 1994.

Selker, J. S., L. Graff, and T. Steenhuis, Noninvasive time domain reflectometry moisture measurement probe, *Soil Sci. Soc. Am. J., 57*, 934–936, 1993.

Topp, G., J. Davis, and A. Annan, Electromagnetic determination of soil water content: Measurements in coaxial transmission lines, *Water Resour. Res., 16*(3), 574–582, 1980.

Topp, G., J. Davis, and A. Annan, Electromagnetic determination of soil water content using TDR, I, Applications to wetting fronts and steep gradients, *Soil Sci. Soc. Am. J., 46*, 672–678, 1982.

Van Beck, L. K. H., Dielectric behavior of heterogeneous systems, *Prog. Dielectr., 7*, 69–114, 1965.

Xu, X., R. Boehm, and R. Venkatasubramanian, Determination of water content in unsaturated flow experiments using TDR and capacitance, in *Proceedings of the International High Level Nuclear Waste Management Conference*, pp. 1051–1057, Am. Nucl. Soc., La Grange Park, Ill./Am. Soc. of Civ. Eng., New York, 1993.

Zegelin, S., I. White, and D. R. Jenkins, Improved field probes for soil water content and electrical conductivity measurement using time domain reflectometry, *Water Resour. Res., 25*(11), 2367–2376, 1989.

R. F. Boehm, Department of Mechanical Engineering, University of Nevada, Las Vegas, NV 89154.

S. V. Maheshwarla and R. Venkatasubramanian, Department of Electrical and Computer Engineering, 4505 Maryland Parkway, Box 454026, University of Nevada, Las Vegas, NV 89154. (e-mail: venkat@univ.edu)

(Received September 15, 1994; revised February 28, 1995; accepted March 4, 1995.)